

## Convective Nature of Sunspot Penumbra Filaments: Discovery of Downflows in the Deep Photosphere

Jayant Joshi<sup>1,2</sup>, A. Pietarila<sup>1,3</sup>, J. Hirzberger<sup>1</sup>, S. K. Solanki<sup>1,4</sup>, R. Aznar Cuadrado<sup>1</sup> and L. Merenda<sup>1</sup>

<sup>1</sup> *Max-Planck-Institute für Sonnensystemforschung, Max-Planck-Str. 2, 37191 Katlenburg-Lindau, Germany*

<sup>2</sup> *Institut für Geophysik und Extraterrestrische Physik, Technische Universität Braunschweig, Braunschweig, Germany*

<sup>3</sup> *National Solar Observatory, 950 N. Cherry Avenue, Tucson, AZ 85719, USA*

<sup>4</sup> *School of Space Research, Kyung Hee University, Yongin, Gyeonggi Do, 446-701, Korea*

joshi@mps.mpg.de

### ABSTRACT

We study the velocity structure of penumbral filaments in the deep photosphere to obtain direct evidence for the convective nature of sunspot penumbrae. A sunspot was observed at high spatial resolution with the 1-m Swedish Solar Telescope in the deep photospheric C 15380 Å absorption line. The Multi-Object Multi-Frame Blind Deconvolution (MOMFBD) method is used for image restoration and straylight is filtered out. We report here the discovery of clear redshifts in the C 15380 Å line at multiple locations in sunspot penumbral filaments. For example, bright head of filaments show larger concentrated blueshift and are surrounded by darker, redshifted regions, suggestive of overturning convection. Elongated downflow lanes are also located beside bright penumbral fibrils. Our results provide the strongest evidence yet for the presence of overturning convection in penumbral filaments and highlight the need to observe the deepest layers of the penumbra in order to uncover the energy transport processes taking place there.

*Subject headings:* Sun:photosphere – Sunspots – Convection

## 1. Introduction

In recent years, indirect evidence for the presence of convection in sunspot penumbral filaments has been growing (e.g., Scharmer 2009). E.g., the twisting motion of penumbral filaments is taken as a signature of overturning convection (Ichimoto et al. 2007; Zakharov et al. 2008; Spruit et al. 2010; Bharti et al. 2010). Using high resolution spectropolarimetric observations, Zakharov et al. (2008) estimated that such motions can provide sufficient heat to the surface layers of the penumbra to explain its relatively high brightness. The correlation of the apparent velocity of the twisting motion with the local brightness of the filaments obtained by Bharti et al. (2010), supports convection as a major source of heat transport in sunspot penumbral filaments. Overturning convection in penumbral filaments is a natural and important feature in three-dimensional MHD simulations of sunspots (Rempel et al. 2009a,b; Rempel 2011). In particular, Rempel et al. (2009b) found upflows along the central axes and downflows at the edges of the filaments. Direct observational evidence for this scenario is, however, so far missing, because downflows have not been measured in the body of a penumbra, although the twisting filaments provide indirect support. The simulations indicate that the convective structures and motions are restricted to the subsurface and surface layers. Since most spectral lines used for diagnostic purposes sample mid-photospheric heights, this may explain why it has not been possible to obtain direct evidence of overturning convection in penumbral filaments (see, e.g., Franz & Schlichenmaier 2009; Bellot Rubio et al. 2010). In particular, downflows at the sides of penumbral filaments have not been reported.

In this study we probe the deep layers of the photosphere in search of such downflows by analyzing high resolution observations in C I 5380.3 Å, obtained at the 1-m Swedish Solar Telescope. In the quiet Sun, C I 5380.3 Å has a mean formation height of around 40 km above the continuum optical depth  $\tau_c = 1$  at 500 nm (Stuereburg & Holweger 1990) making it ideal for this purpose.

## 2. Observation and Data Reduction

We observed a decaying sunspot with a one-sided penumbra in active region NOAA 11019 (cf. Fig. 1) with the 1-meter Swedish Solar Telescope (SST) on 2009, June 02. The center of the field of view (FOV) was located at  $\mu = 0.84$  (heliocentric angle = 32.7°). During the observations the seeing conditions were good to excellent, with only few interruptions by poorer seeing.

We carried out consecutive spectral scans of the photospheric C I 5380.3 Å, Fe I 5250.2 Å and the chromospheric Ca II 8542 Å spectral lines using the CRISP imaging spectropolarimeter.

Here we analyze only the C I 5380.3 Å line<sup>1</sup>. Two liquid crystal variable retarders, used to modulate the light beam, and two 1k×1k-pixel Sarnoff CCD cameras, mounted behind a polarizing beam splitter, were used to record the full Stokes vectors at each spectral position. A third CCD camera was used to record broad-band images. All three cameras were synchronized in order to allow post-facto image restoration. We recorded the C I 5380 Å line at 8 wavelength positions ( $\lambda - \lambda_0 = [-300, -120, -80, -40, 0, 40, 80, 120]$  mÅ). Scanning the line in all four Stokes parameters required 14 s for the C I 5380.3 Å line. The cadence of these observations, including the Fe I 5250.2 Å and Ca II 8542 Å scans (not considered in the present study) is 29 s.

To achieve near diffraction limited spatial resolution (0.14"), images were reconstructed using the Multi-Object Multi-Frame Blind Deconvolution (MOMFBD) method (van Noort et al. 2005; Löfdahl 2002). Images observed in C I 5380 Å and Fe I 5250 Å were aligned with sub-pixel accuracy by cross-correlating the corresponding continuum images. We determined Doppler velocities by fitting a Gaussian function to the C I line. Due to the low Landé factor ( $g_{\text{eff}} = 1$ , Solanki & Brigljevic 1992) and large thermal width of the line, this is an acceptable approach even in a sunspot. The good quality of the Gaussian fit throughout the penumbra suggests that the line is unblended there, unlike in the umbra (see Sect. 3). Another reason for expecting that the line is unblended (or at the most rather weakly blended) in the penumbra is that the line strength increases strongly with temperature, a nearly unique property of C I lines among photospheric spectral lines.

The resulting velocity maps show variations of the mean quiet Sun velocities across the FOV caused by the absolute wavelength positions varying across the FOV due to cavity errors of the etalons of CRISP. These wavelength shifts are smeared out in a continuously changing manner due to varying seeing conditions. The applied calibration data (flat fields), which are well defined in pixel space, are no longer connected to pixel space of the science data after restoration (Schnerr et al. 2010). Therefore, the cavity errors cannot be fully removed with the flat fields. The absolute wavelength shifts caused by the cavity errors are wavelength dependent and the residuals after correction for flat-field cavity shifts are much higher in the 5380 Å band than in the 6300 Å and 6560 Å bands, used in previous studies carried out with CRISP (see, e.g., Scharmer et al. 2008; Rouppe van der Voort et al. 2010; Ortiz et al. 2010). Since the residual wavelength shifts across the FOV are expected to be large-scale, however, they do not rule out a study of penumbral fine structure. In order to determine a confidence level of the resulting absolute velocity reference point of the Doppler velocities we selected 19 quiet Sun subfields of 6" × 6" size throughout the FOV, indicated by the colored squares in Fig. 1. The relative quietness of the selected subfields was assured by a threshold value (4 %) of spectrally averaged absolute circular polarization<sup>2</sup> in the line

---

<sup>1</sup>The Fe I 5250.2 Å line is used only to identify "quiet Sun" locations, where the polarization signal in this line is below a given threshold.

<sup>2</sup>A full polarimetric model of the SST in the observed spectral range is not available so far. Therefore, we are not

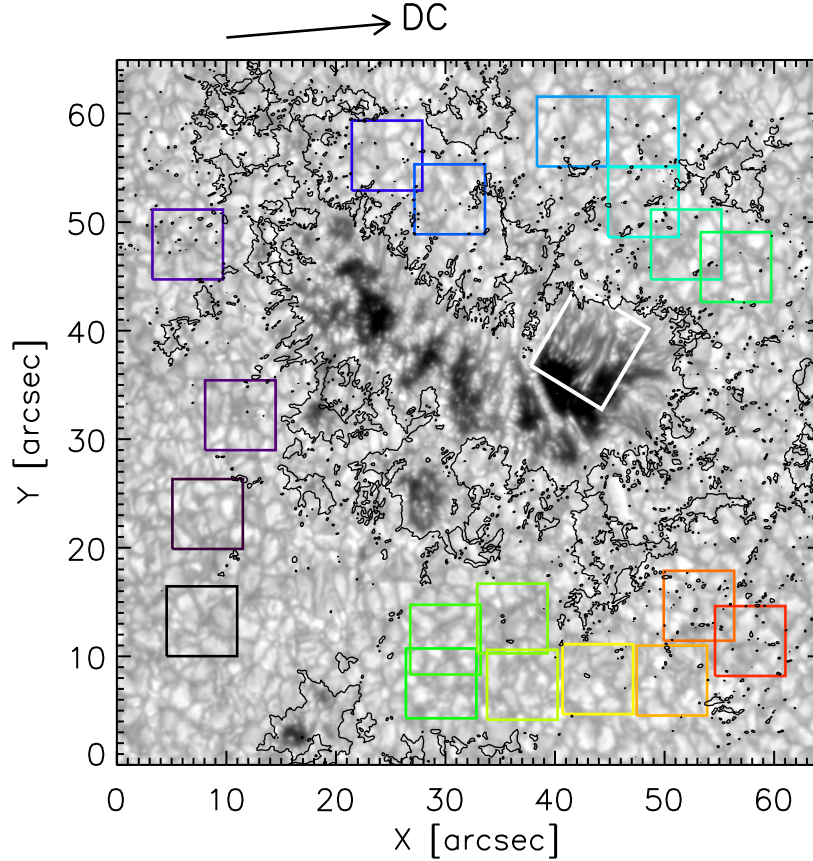


Fig. 1.— Continuum image at  $5380 \text{ \AA}$  of the decaying sunspot with a penumbra mainly on one side. Black contours outline regions where the absolute circular polarization averaged over the two line wings ( $\pm 40 \text{ m\AA}$  from average line center) of the  $\text{Fe I } 5250 \text{ \AA}$  line is greater than 4 %. Colored boxes ( $6'' \times 6''$ ) show the different quiet Sun fields used to calculate the velocity reference value. The thick white rectangle marks the portion of the image shown in Fig. 5 in detail.

wings ( $\pm 40 \text{ m\AA}$  from average line center) of  $\text{Fe I } 5250.2 \text{ \AA}$ . We calculated mean Doppler velocities of  $\text{C I } 5380 \text{ \AA}$  by spatially averaging the line profiles in each subfield and repeated this procedure for all the observed sequences, i.e., over 20 min. The results from this procedure are shown in Fig. 2. The velocity in each subfield fluctuates randomly, but does not exhibit a systematic variation with time. In order to get a mean quiet Sun velocity reference, we fitted a Gaussian to the velocity distribution and obtained a mean value of  $-480 \text{ m s}^{-1}$  and a full width at half maximum (FWHM) of  $580 \text{ m s}^{-1}$  for the  $\text{C I } 5380 \text{ \AA}$  line, i.e., the residual uncertainty ( $1\sigma$ ) in the absolute

---

able to carry out a complete correction for instrumental cross-talk and the displayed polarimetric information can be considered only as a rough estimate of the magnetic field structure in the FOV.

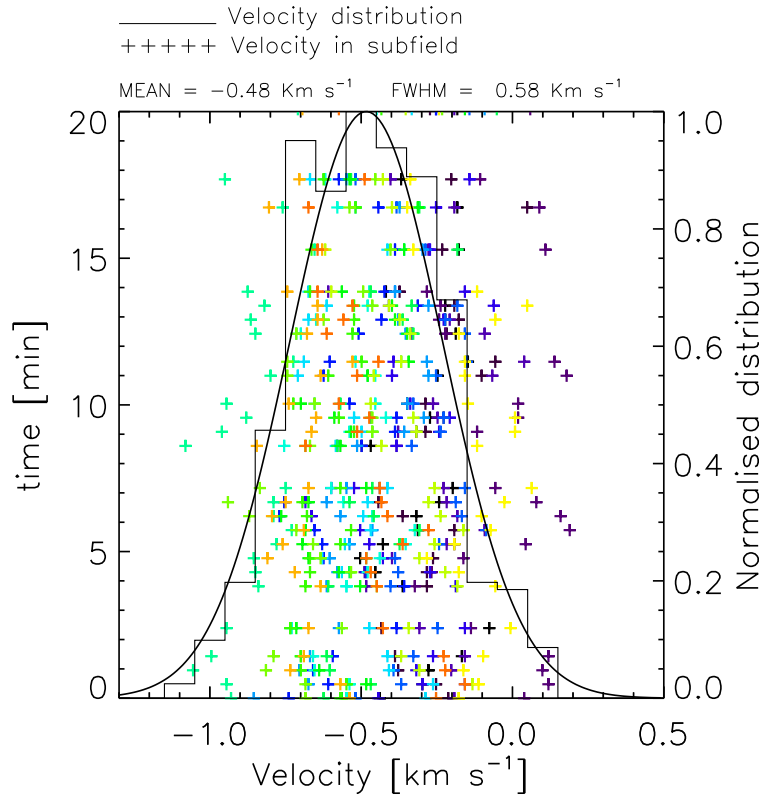


Fig. 2.— Mean velocities obtained from average line profiles of the subfields shown in Fig. 1 (abscissa) vs. time of observation relative to the time of the first recording (ordinate). Colors correspond to the subfields bounded by squares of with the same colors in Fig. 1. The velocity distribution and a Gaussian fit are represented by solid lines.

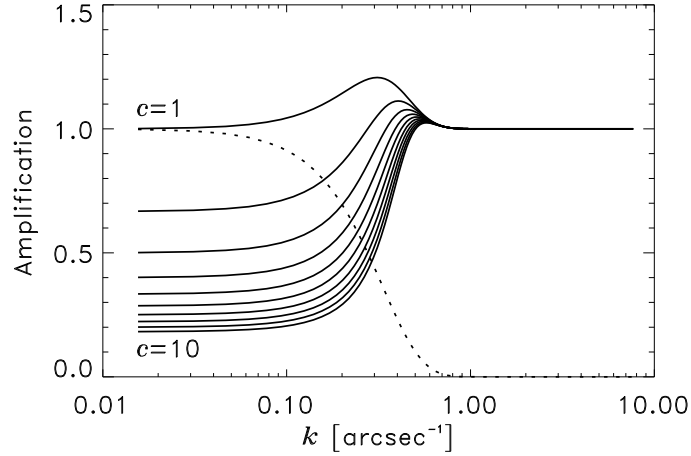


Fig. 3.— Applied filter to deconvolve straylight. The solid curves denote filter shapes for  $c = 1 \dots 10$  (see Eq. (1)). The dotted curve represents the *MTF*, i.e., the Fourier transform of a Gaussian of  $1.6''$  width.

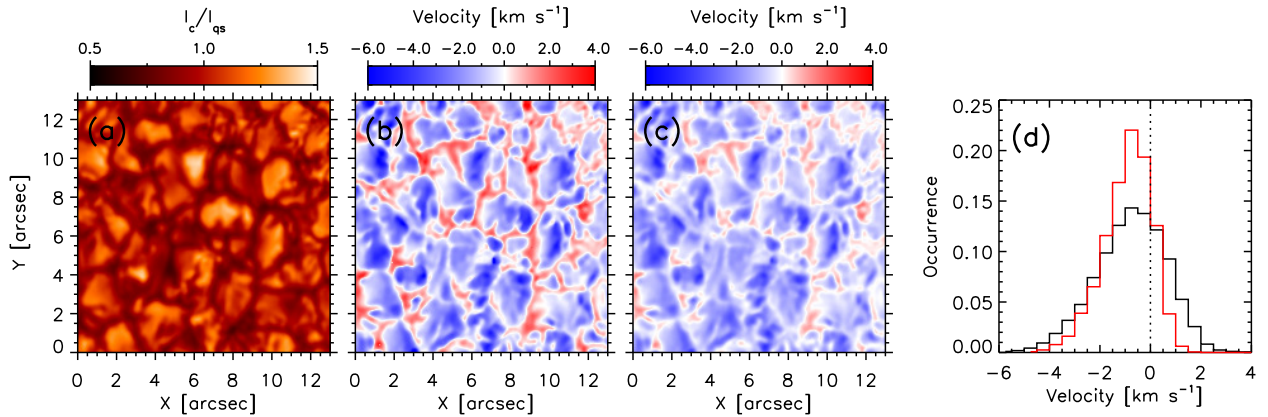


Fig. 4.— Panels (a) and (b) display a quiet Sun continuum map near  $C \text{ I } 5380.0 \text{ \AA}$  and the corresponding Doppler map after straylight removal, respectively. Panel (c) shows, for comparison, the Doppler map before straylight removal while histograms of Doppler velocity before (red) and after (black) straylight removal are plotted in panel (d)

Doppler velocities is  $\pm 248 \text{ m s}^{-1}$ . After applying this procedure, the mean values of the obtained velocity maps are calibrated for a convective blueshift of  $-922 \text{ m s}^{-1}$  for C I 5380.3 Å (de La Cruz Rodríguez et al. 2011). For the further analysis we selected the scan of C I 5380.3 Å made under the best seeing conditions.

## 2.1. Straylight Correction

Ground-based observations are strongly affected by straylight, so that, e.g., contrasts are significantly lower than in data recorded above the Earth’s atmosphere (see, e.g., Danilovic et al. 2008; Hirzberger et al. 2010). We also expect the velocity to be reduced through straylight. The amount of straylight and the shape of the corresponding straylight point spread function is strongly dependent on the seeing conditions and on the instrument design. The straylight point spread functions can be approximated from fitting observations of the solar limb (aureolas, see, e.g., Sobotka et al. 1993) or from fitting the profiles of planetary limbs during transits (see, e.g., Bonet et al. 1995; Mathew et al. 2009; Wedemeyer-Böhm & Rouppe van der Voort 2009). Since we do not have these auxiliary data, we applied a rough estimation, assuming that the biggest amount of the straylight stems from regions within  $1.6''$  around the respective positions (approximately the ten-fold of the spatial resolution of the data), i.e., we approximated the straylight point spread function with a Gaussian of  $1.6''$  width. For deconvolving the images we used the Wiener filter given in Sobotka et al. (1993) and applied a slight modification, so that it has the shape

$$F(k) = \frac{1}{c} \frac{MTF(k) + 1}{MTF(k)^2 + 1/c}, \quad (1)$$

where MTF is the modulation transfer function (the modulus of the Fourier transform of the point spread function),  $k$  is the spatial wavenumber and  $c$  is a free parameter which defines the straylight contribution that has to be deconvolved.  $F(k)$  for different choices of  $c$  is plotted in Fig. 3. The advantage of the present form of the filter compared to the one used in Sobotka et al. (1993) is that it converges to unity for large  $k$ , i.e., it does not affect the small-scale structures of the images.

In the present study the value of parameter  $c$  has been chosen equal to 2.0, so that the resulting quiet Sun rms image contrast for the continuum point (at  $\lambda = \lambda_0 - 300 \text{ mÅ}$ ) of the best scan increases from 8.5% in the original image to 13.0% in the deconvolved image, which is closer to, but still somewhat smaller than the contrast obtained from data at a similar wavelength that are much less contaminated by straylight (continuum at 5250.4 Å in IMAx/Sunrise observations, see Martínez Pillet et al. 2011). We finally used this conservative choice, although we also tested other straylight functions, including broad Gaussians with widths up to  $16''$ . The results of using stronger straylight removal (larger  $c$ ) or broader Gaussians, remained similar, but provided stronger downflows and, for larger  $c$ , also stronger contrast. Stronger straylight removal also led to bigger

scatter in the velocities and somewhat more distorted line profiles, which was another reason to keep to the conservative value of straylight.

We selected a  $13'' \times 13''$  field in the quiet Sun to compare velocities before and after straylight removal. Results are shown in Fig. 4. The redshift in inter-granular lanes increases disproportionately through straylight removal (see panels (b), (c) and (d) of Fig. 4. Downflows are particularly affected by straylight because they are narrower and are present in darker features. The fact that the downflows remain weaker than upflows also after our standard straylight removal confirms that we have been conservative in the removed amount of straylight.

### 3. Results

Panels (a) and (c) of Fig. 5 show a portion of the observed penumbra as seen in the continuum intensity (at  $\lambda = \lambda_0 - 300 \text{ m\AA}$ ), before and after straylight removal, respectively. The corresponding maps of Doppler velocity are plotted in panels (b) and (d). Obviously both blue- and redshifts are present in the penumbra, in particular after straylight removal. A striking feature in Fig. 5b is the localized patches of strong blueshift, up to  $3.3 \text{ km s}^{-1}$ , coinciding with the bright heads of penumbral filaments. These bright heads are surrounded by lanes of gas nearly at rest or slightly redshifted. In panel (b) significant redshifts are visible only at two locations, once at the side of a filament reaching into the umbra (at  $x = 6''$  and  $y = 1''$ ) and once, rather weakly around the bright and strongly blueshifted head of a filament (at  $x = 6.5''$  and  $y = 4.5''$ ).

A number of new redshifted patches are found in the Doppler map after straylight removal (panel d), appearing dominantly at locations previously seemingly at rest in panel (b). We have grayed out areas where intensity is below 0.6 times that of the quiet Sun, because  $\chi^2$  values of the Gaussian fits to the line profiles are high in these areas since the line is very weak there and possibly blended (as suggested by the fact that we obtain mainly strong blueshifts in the umbra contrary to all previous studies based on other spectral lines). Redshifts (largest value  $2.0 \text{ km s}^{-1}$ ) show a tendency to be located in dark regions, as can be judged by considering the white contours in panel (c). These contours outline the redshift of panel (d). Redshifts are now found clearly around the head of multiple filaments (e.g., at  $x = 2''$  and  $y = 3''$  and around the filaments protruding into the umbra). Narrow redshifted areas are also found in the middle and outer penumbra beside and between bright filaments.

Clearly, in the lower photosphere redshifts are present at many different locations in the penumbra. We expect that only a part of redshifted features actually present in the penumbra has been detected.

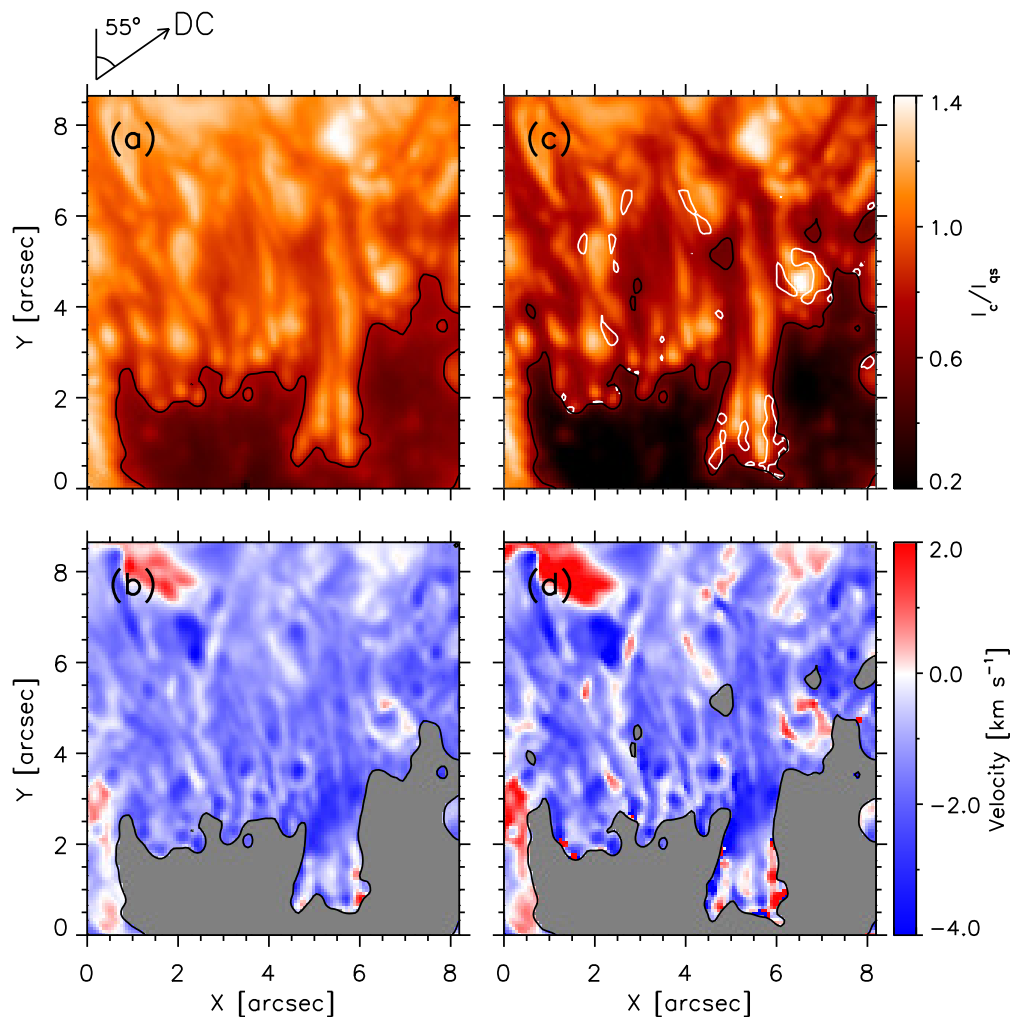


Fig. 5.— (a) Continuum intensity map in the penumbral region of the observed sunspot obtained from the C I 5380 Å line. The displayed region is marked by the thick white rectangle in Fig. 1. (b) the corresponding Doppler velocity, (c) continuum intensity map after straylight removal, (d) Doppler velocity after straylight removal. Gray color encircled by black contours in panels (b) and (d) represent areas where continuum intensity is less than  $0.6 I_{qs}$ . White contours in panel (c) outline penumbral downflows and show that these are located in darker parts of the penumbra. The arrow above panel (a) indicates the direction toward solar disk center.

#### 4. Discussion

We have provided the first direct measurements of downflows (reaching  $2.0 \text{ km s}^{-1}$ ) in the body of a penumbra. The studied sunspot, located at  $\mu = 0.84$ , had only a partial penumbra, on the disk-center side of the spot, so that all well-defined filaments partially point to disk center. Hence the Evershed flow contributes a blueshift, so that redshifts in Fig. 5d must be caused by downflows (or inflow, which appears rather unlikely, however).

The  $C \text{ I } 5380 \text{ \AA}$  line reveals a highly structured velocity pattern, with large variations in velocity around the head of filaments. Typical blueshift of  $3 \text{ km s}^{-1}$  found in the bright head of the filaments, surrounded by gas displaying redshift (after straylight removal) or no shift. We interpret them as strong localized upflows of hot gas in the head of the filaments following Rimmele & Marino (2006),, but cannot rule out that they are due to Evershed flow. A fraction of this gas starts moving along the axis of the filaments and forming the Evershed flow (Scharmer et al. 2008). The rest of the gas moves to the sides of the filaments and flows downward. Further downflows are found alongside bright filaments in the middle and outer part of this penumbra. Such downflows have been predicted by models of penumbral convection (e.g., Rempel et al. 2009a,b; Scharmer & Spruit 2006). Earlier observational studies have provided only indirect evidence for such downflows (Ichimoto et al. 2007; Zakharov et al. 2008; Bharti et al. 2010; Spruit et al. 2010).

The velocity at the heads of the filaments reaches values up to  $3.3 \text{ km s}^{-1}$ , interpreted here as upflows, agrees with earlier observational results (Rimmele 1995; Rimmele & Marino 2006; Hirzberger & Kneer 2001; Hirzberger et al. 2005). Such upflows are also consistent with the moving flux tube model presented by Schlichenmaier et al. (1998), which predicts an upflow of  $4 \text{ km s}^{-1}$  at the footpoints of the penumbral filaments, but equally with the interpretation of Scharmer et al. (2008) that the Evershed flow is a horizontal flow component of overturning convection. In recent years, convection has become an important candidate to explain the heat transport in penumbrae. Based on the observed  $1 \text{ km s}^{-1}$  upflow at the axis of the filament in the upper layers of the photosphere, Zakharov et al. (2008) estimated the heat transport by convection in the penumbra to be sufficient for maintaining the brightness of the penumbra. The upflows up to  $3.3 \text{ km s}^{-1}$  in the bright heads of penumbral filaments with downflows at the filament sides, found in the present study, and the coincidence of the strongest upflows with bright filaments and downflows with dark filaments strongly support that the heat transport in the penumbra is accomplished by convection.

In the outer sections of penumbral filaments (i.e. further from the umbra) we found maximum blueshifts of up to  $3.0 \text{ km s}^{-1}$ . If we assume that of this blueshift is due to the Evershed effect, its projection in the direction of disk center and parallel to solar surface gives  $8.5 \text{ km s}^{-1}$  of radial outflow. This upper limit agrees well with results from the simulation by Rempel (2011) which shows Evershed flow speeds above  $8 \text{ km s}^{-1}$  near  $\tau = 1$ .

The true strength of the penumbral downflows are expected to be larger than found here for the following reasons. For the same reasons we expect a number of the locations still seemingly at rest, in reality be filled with downflowing gas.

1. Incomplete removal of straylight. We have been rather conservative when removing straylight, since the assumed granular contrast of 13% is smaller than values found by Mathew et al. (2009) at 5550 Å from Hinode and Martínez Pillet et al. (2011) at 5250 Å from SUNRISE.
2. A blueshift imposed by the LOS-component of the Evershed flow. The major axis of most of the filaments makes an angle of  $\sim 55^\circ$  with the line joining the sunspot and the disk center. Thus, we expect radial outflow due to Evershed effect to contribute as  $V_{LOS} = V_E \sin \theta \cos 55^\circ = 0.35V_E$  (where  $V_E$  represents the Evershed velocity) to the LOS velocity. The Evershed flow probably hides a significant amount of the redshift due to downflowing gas (cf. Bharti et al. 2011).
3. The geometry of the filaments. As proposed by Zakharov et al. (2008) the penumbral  $\tau = 1$  surface is strongly corrugated, so that we see the disk center side of the filaments more clearly than the other side (see their Fig. 4). Hence, in our sunspot we might expect the downflows to be better visible on the diskward side of a filament where they may be partly covered by the filament lying in front of them. This interpretation is supported by the fact that the strongest downflows are found on the diskward side of a filament extending into the umbra, where no other filament can block the view of its edge.

In summary, we report the discovery of downflows at the edges of bright penumbral filaments in the deep photospheric layers. Such downflows are expected for overturning convection in the penumbra.

This work has been partially supported by WCU grant No. R31-10016 funded by the Korean Ministry of Education, Science and Technology. The Swedish 1-m Solar Telescope is operated on the island of La Palma by the Institute for Solar Physics of the Royal Swedish Academy of Sciences in the Spanish Observatorio del Roque de los Muchachos of the Instituto de Astrofísica de Canarias. JJ acknowledges a PhD fellowship of the International Max Planck Research School on Physical Processes in the Solar System and Beyond.

## REFERENCES

Bellot Rubio, L. R., Schlichenmaier, R., & Langhans, K. 2010, ApJ, 725, 11

- Bharti, L., Schüssler, M., & Rempel, M. 2011, ApJ (submitted)
- Bharti, L., Solanki, S. K., & Hirzberger, J. 2010, ApJ, 722, L194
- Bonet, J. A., Sobotka, M., & Vazquez, M. 1995, A&A, 296, 241
- Danilovic, S., Gandorfer, A., Lagg, A., Schüssler, M., Solanki, S. K., Vögler, A., Katsukawa, Y., & Tsuneta, S. 2008, A&A, 484, L17
- de La Cruz Rodríguez, J., Kiselman, D., & Carlsson, M. 2011, A&A, 528, A113
- Franz, M. & Schlichenmaier, R. 2009, A&A, 508, 1453
- Hirzberger, J., Feller, A., Riethmüller, T. L., Schüssler, M., Borrero, J. M., Afram, N., Unruh, Y. C., Berdyugina, S. V., Gandorfer, A., Solanki, S. K., Barthol, P., Bonet, J. A., Martínez Pillet, V., Berkefeld, T., Knölker, M., Schmidt, W., & Title, A. M. 2010, ApJ, 723, L154
- Hirzberger, J. & Kneer, F. 2001, A&A, 378, 1078
- Hirzberger, J., Stangl, S., Gersin, K., Jurčák, J., Puschmann, K. G., & Sobotka, M. 2005, A&A, 442, 1079
- Ichimoto, K., Suematsu, Y., Tsuneta, S., Katsukawa, Y., Shimizu, T., Shine, R. A., Tarbell, T. D., Title, A. M., Lites, B. W., Kubo, M., & Nagata, S. 2007, Science, 318, 1597
- Löfdahl, M. G. 2002, in Proc. SPIE, Vol. 4792, Image Reconstruction from Incomplete Data II, ed. P. J. Bones, M. A. Fiddy, & R. P. Millane, 146–155
- Martínez Pillet, V., Del Toro Iniesta, J. C., Álvarez-Herrero, A., Domingo, V., Bonet, J. A., González Fernández, L., López Jiménez, A., Pastor, C., Gasent Blesa, J. L., Mellado, P., Piqueras, J., Aparicio, B., Balaguer, M., Ballesteros, E., Belenguer, T., Bellot Rubio, L. R., Berkefeld, T., Collados, M., Deutsch, W., Feller, A., Girela, F., Grauf, B., Heredero, R. L., Herranz, M., Jerónimo, J. M., Laguna, H., Meller, R., Menéndez, M., Morales, R., Orozco Suárez, D., Ramos, G., Reina, M., Ramos, J. L., Rodríguez, P., Sánchez, A., Uribe-Patarroyo, N., Barthol, P., Gandorfer, A., Knoelker, M., Schmidt, W., Solanki, S. K., & Vargas Domínguez, S. 2011, Sol. Phys., 268, 57
- Mathew, S. K., Zakharov, V., & Solanki, S. K. 2009, A&A, 501, L19
- Ortiz, A., Bellot Rubio, L. R., & Rouppe van der Voort, L. 2010, ApJ, 713, 1282
- Rempel, M. 2011, ApJ, 729, 5
- Rempel, M., Schüssler, M., Cameron, R. H., & Knölker, M. 2009a, Science, 325, 171

- Rempel, M., Schüssler, M., & Knölker, M. 2009b, *ApJ*, 691, 640
- Rimmele, T. & Marino, J. 2006, *ApJ*, 646, 593
- Rimmele, T. R. 1995, *A&A*, 298, 260
- Roupe van der Voort, L., Bellot Rubio, L. R., & Ortiz, A. 2010, *ApJ*, 718, L78
- Scharmer, G. B. 2009, *Space Science Reviews*, 144, 229
- Scharmer, G. B., Narayan, G., Hillberg, T., de la Cruz Rodriguez, J., Löfdahl, M. G., Kiselman, D., Sütterlin, P., van Noort, M., & Lagg, A. 2008, *ApJ*, 689, L69
- Scharmer, G. B. & Spruit, H. C. 2006, *A&A*, 460, 605
- Schlichenmaier, R., Jahn, K., & Schmidt, H. U. 1998, *A&A*, 337, 897
- Schnerr, R. S., de la Cruz Rodriguez, J., & van Noort, M. 2010, *A&A* (submitted)
- Sobotka, M., Bonet, J. A., & Vazquez, M. 1993, *ApJ*, 415, 832
- Solanki, S. K. & Brigljevic, V. 1992, *A&A*, 262, L29
- Spruit, H. C., Scharmer, G. B., & Löfdahl, M. G. 2010, *A&A*, 521, A72
- Stuerenburg, S. & Holweger, H. 1990, *A&A*, 237, 125
- van Noort, M., Roupe van der Voort, L., & Löfdahl, M. G. 2005, *Sol. Phys.*, 228, 191
- Wedemeyer-Böhm, S. & Roupe van der Voort, L. 2009, *A&A*, 503, 225
- Zakharov, V., Hirzberger, J., Riethmüller, T. L., Solanki, S. K., & Kobel, P. 2008, *A&A*, 488, L17